5

Simulation of Bonded Joints Failure using Progressive Mixed-Mode Damage Models

M.F.S.F. de Moura and J.A.G. Chousal

Faculty of Engineering, University of Porto, Porto, Portugal

Abstract

In the most recent years, structural applications of bonded joints have increased remarkably owing to their several advantages relative to other joining methods. As a consequence, the development of improved models to provide design efficiency and, at the same time, increase the confidence of designers acquires special relevancy. Recent developments considering cohesive and continuum mixed-mode damage models have demonstrated that these methods are able to deal with several details inherent to mechanical behaviour of bonded joints. Both methods allow simulation of damage initiation and propagation by combining classical strength of materials approaches with fracture mechanics concepts.

In this work, several different mixed-mode cohesive laws adapted to different types of adhesives mechanical behaviour are presented and discussed. Effectively, while mechanical behaviour of brittle or moderately ductile adhesives is well simulated by means of the simple bilinear cohesive law, adhesives with pronounced ductile behaviour require more sophisticated cohesive laws. The aspects regarding determination of some cohesive parameters are also given special attention in the present paper. A continuum mixed-mode damage model is also presented using the bilinear softening cohesive law. This model is advantageous since properties degradation takes place inside solid elements used to simulate the adhesive, which allows the evaluation of specific issues like the influence of asymmetric propagation on joint mechanical behaviour in a more realistic manner. Important conclusions about advantages and drawbacks of both methodologies are drawn.

Keywords: Bonded joints, cohesive damage model, continuum damage model, mixed-mode

5.1   Introduction

The application of bonded joints in critical structures has been increasing during the most recent years owing to their several advantages relative to alternative joining methods. This necessitates the development of adequate design methods accounting for specificities of damage initiation and growth which are not included in classical design methods. In fact, methods based on strength of materials approaches [1–3] show difficulties in dealing with geometrical singularities, which are usually present in bonded joints. In these cases, stresses tend to infinity in a linear elastic analysis. This problem can be observed in finite element analysis, when stresses at the singularity point increase with the mesh refinement and convergence cannot be reached. To overcome this problem the stresses obtained numerically can be evaluated at a characteristic distance from the singularity point or averaged over a distance in order to evaluate the occurrence of failure [4–6]. However, the lack of a physical meaning of this characteristic distance makes it difficult to establish a predictive methodology independent of a parameter which is a function of type of loading, materials involved and joint geometry. Fracture mechanics based methods [7–8] can also be applied to evaluate joint's strength. In this case, the presence of a defect in the material is assumed. The objective is to verify whether the defects can induce failure or, during the predicted structure life, they can propagate stably maintaining their dimensions less than the critical size. Hence, it can be concluded that fracture mechanics based criteria are more adequate for damage propagation instead of its onset. On the other hand, the definition of the initial crack length and its location can be viewed as two main drawbacks intrinsic to this approach.

As a result, the development and application of damage onset and propagation methods to bonded joints design can be viewed as a fundamental task when dealing with design of critical structures. In this context, cohesive and continuum damage models can be viewed as valuable alternatives to classical approaches described above. Both of these are based on stress criteria to deal with damage onset and fracture criteria to simulate damage growth. The advantage of this strategy relies in the fact that stress-based methods are adequate to predict damage onset, and fracture mechanics is suitable for crack propagation modelling. Effectively, by combining these two types of criteria it is not necessary to consider an initial

flaw as it is done in pure fracture mechanics methods, and mesh dependency problems in finite element analysis are overcome.

5.2   Cohesive Damage Model

Cohesive damage models are usually based on interface finite elements connecting plane or three-dimensional solid elements [9–11]. The interface elements should be placed at the planes where damage is prone to occur which means that critical regions must be identified in advance. In bonded joints these regions can be identified as being the interfaces between the adhesive and the adherends as well as in the middle of the adhesive. Interface elements include a softening relationship between stresses and relative displacements between element faces in order to simulate smooth material properties degradation. Different cohesive damage laws have been applied in the context of bonded joints [12–14]. The bilinear cohesive law with a linear softening relationship [12] is appropriate when brittle or moderately ductile adhesives are used. In the case of pronounced ductility, the trapezoidal cohesive law whose plateau accounts for adhesive plasticization [15] is more adequate.

In the following a trapezoidal cohesive mixed-mode I+II damage model (Figure 5.1) appropriate for bonded joints is presented. Although this type of law is particularly adequate to characterize fracture of ductile adhesives, the presented formulation comprises the bilinear law since it is a particular case of the trapezoidal one. In fact, the trapezoidal law transforms into the bilinear one when the plateau vanishes. The model establishes a constitutive softening
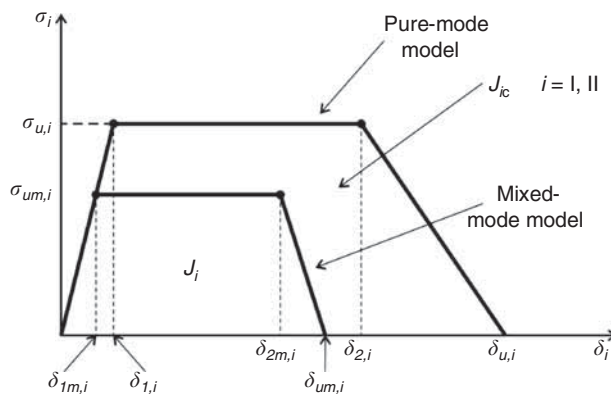
Figure 5.1 Pure and mixed-mode I+II cohesive damage model.

law relating stresses (σ) and relative displacements (δ$_r$) between homologous points of interface finite elements connecting solid elements. In the linear elastic regime, i.e., before the occurrence of any damage

$$\sigma = E\delta_r \tag{5.1}$$

where E is the interface stiffness diagonal matrix (e_i, i = I, II). In order to account indirectly for the presence of the adhesive on the joint stiffness, the parameters e_i are defined as being the ratio between the Young's (mode I) or shear modulus (mode II), and adhesive thickness. In the pure-mode damage model, damage onset takes place when the relative displacement reaches $\delta_{1,i}$ and the constitutive equation becomes

$$\sigma = (I - D)E\delta_r \tag{5.2}$$

being I is the identity matrix and D is a diagonal matrix containing, in the position corresponding to mode i (i=I, II), the damage parameter, d. In the plateau region the parameter damage can be defined as

$$d = 1 - \frac{\delta_{1,i}}{\delta_i} \tag{5.3}$$

where $\delta_{1,i}$ (i= I, II) is obtained from the initial stiffness (e_i) and local cohesive strength in mode i, $\sigma_{u,i}$. In the stress softening part of the law,

$$d = 1 - \frac{\delta_{1,i}(\delta_{u,i} - \delta_i)}{\delta_i(\delta_{u,i} - \delta_{2,i})} \tag{5.4}$$

The relative displacement corresponding to second inflexion point can be obtained by an inverse method following an iterative procedure in order to obtain agreement between numerical and experimental load-displacement curves from the fracture test used to characterize the bonded joint. The relative displacement corresponding to complete failure ($\delta_{u,i}$) results from the respective fracture energy J_{ic}, which is defined by the area defined by the softening law (Figure 5.1), thus leading to

$$\delta_{u,i} = \frac{2J_{ic}}{\sigma_{u,i}} - \delta_{2,i} + \delta_{1,i} \tag{5.5}$$

Since bonded joints usually are under mixed-mode (I+II) loading, an extension of the pure-mode damage model was developed (Figure 5.1). A quadratic stress criterion is used to simulate damage initiation

$$\left(\frac{\sigma_{\mathrm{I}}}{\sigma_{u,\mathrm{I}}}\right)^2 + \left(\frac{\sigma_{\mathrm{II}}}{\sigma_{u,\mathrm{II}}}\right)^2 = 1 \text{ if } \sigma_{\mathrm{I}} > 0$$

$$\sigma_{\mathrm{II}} = \sigma_{u,\mathrm{II}} \qquad if \ \sigma_{\mathrm{I}} \le 0 \tag{5.6}$$

where σ_i and $\sigma_{u,i}$ (i=I, II) represent, respectively, the stresses and local cohesive strengths in each mode. It is assumed that normal compressive stresses do not induce damage. Taking into account the relation between stresses and relative displacements (Eq. 5.1), the first Eq. 5.6 can be rewritten as

$$\left(\frac{\delta_{1m,\mathrm{I}}}{\delta_{1,\mathrm{I}}}\right)^2 + \left(\frac{\delta_{1m,\mathrm{II}}}{\delta_{1,\mathrm{II}}}\right)^2 = 1 \tag{5.7}$$

where $\delta_{1m,i}$ (i = I, II) are the components of relative displacements in each mode leading to damage initiation. Utilizing the equivalent mixed-mode displacement

$$\delta_m = \sqrt{\delta_{\mathrm{I}}^2 + \delta_{\mathrm{II}}^2} \tag{5.8}$$

and the mixed-mode ratio

$$\beta = \frac{\delta_{\mathrm{II}}}{\delta_{\mathrm{I}}} \tag{5.9}$$

the equivalent mixed-mode relative displacement at the onset of the softening process ($\delta_{1m} = \sqrt{\delta_{1m,\mathrm{I}}^2 + \delta_{1m,\mathrm{II}}^2}$) is obtained by combining Eqs. 5.7–5.9 as:

$$\delta_{1m} = \delta_{1,\mathrm{I}}\delta_{1,\mathrm{II}} \sqrt{\frac{1 + \beta^2}{\delta_{1,\mathrm{II}}^2 + \beta^2 \delta_{1,\mathrm{I}}^2}} \tag{5.10}$$

It should be noted that the mixed-mode ratio (Eq. 5.9) is obtained from the current relative displacements which means that β, for a given integration point can change along the softening region during the loading history.

For the second inflexion point corresponding to stress softening onset (δ_{2m}), a relative displacements quadratic criterion

similar to the one considered for the damage initiation point (Eq. 5.7) is used,

$$\left(\frac{\delta_{2m,\mathrm{I}}}{\delta_{2,\mathrm{I}}}\right)^2 + \left(\frac{\delta_{2m,\mathrm{II}}}{\delta_{2,\mathrm{II}}}\right)^2 = 1 \tag{5.11}$$

leading to

$$\delta_{2m} = \delta_{2,\mathrm{I}}\delta_{2,\mathrm{II}}\sqrt{\frac{1+\beta^2}{\delta_{2,\mathrm{II}}^2 + \beta^2\delta_{2,\mathrm{I}}^2}} \tag{5.12}$$

where $\delta_{2\mathrm{m}}$ is the mixed-mode relative displacement at the second inflexion point.

In order to simulate crack propagation the linear fracture energetic criterion is employed

$$\frac{J_{\mathrm{I}}}{J_{\mathrm{Ic}}} + \frac{J_{\mathrm{II}}}{J_{\mathrm{IIc}}} = 1 \tag{5.13}$$

where J_i (i=I, II) represent the energy released in each mode at failure and J_{ic} (i=I, II) the respective critical values. The energies J_i can be obtained from the area of the smaller trapezoid of Figure 5.1

$$J_i = \frac{\sigma_{um,i}}{2}\left(\delta_{2\mathrm{m},i} - \delta_{1\mathrm{m},i} + \delta_{um,i}\right) \tag{5.14}$$

Combining Eqs. 5.1, 5.8, 5.9, 5.14 and 5.13 it can be written

$$\delta_{um} = \frac{2J_{\mathrm{Ic}}J_{\mathrm{IIc}}\left(1+\beta^2\right) - \left(\delta_{2\mathrm{m}} - \delta_{1\mathrm{m}}\right)\delta_{1\mathrm{m}}\left(e_{\mathrm{I}}J_{\mathrm{IIc}} + \beta^2 e_{\mathrm{II}}J_{\mathrm{Ic}}\right)}{\delta_{1\mathrm{m}}\left(e_{\mathrm{I}}J_{\mathrm{IIc}} + \beta^2 e_{\mathrm{II}}J_{\mathrm{Ic}}\right)} \tag{5.15}$$

which corresponds to the equivalent ultimate relative displacement under mixed-mode I+II loading. The damage parameter can now be evaluated using in Eqs. 5.3 and 5.4 the equivalent current relative displacement (Eq. 5.8) and critical mixed-mode relative displacements (Eqs. 5.10, 5.12 and 5.15), instead of the respective pure mode values. The evolution of the damage parameter allows the simulation of a progressive softening which accounts for different failure processes occurring in the vicinity of the crack tip. In fact, in this region, known as the Fracture Process Zone (FPZ), several damage processes take place e.g., plasticity and micro-cracking, which are simulated by this softening law.

5.3   Measurement of Cohesive Parameters

One of the fundamental issues regarding this approach is the estimation of the cohesive parameters intrinsic to each pure mode. Since bonded joints are usually used as thin bonded layers, tests on bulk specimens are not adequate to perform such characterization. Fracture characterization tests (Double Cantilever Beam for pure mode I and End Notched Flexure for pure mode II) can be performed by considering specimens with similar geometric and materials conditions as in the intended application. One of the aspects that can be viewed as critical is the adhesive thickness, which must be the same since some influence on the measured fracture properties has been observed [16].

5.3.1   Double Cantilever Beam (DCB) Test

The DCB is a standardized test (ASTM D3433-99) used to perform fracture characterization of materials under pure mode I loading. The application of the DCB test to bonded joints fracture characterization requires a careful monitoring of adhesive thickness during the manufacturing process and the consideration of a pre-crack length. The application of load (Figure 5.2) induces pure mode I crack growth thus allowing the measurement of the mode I fracture energy.

Two methods are commonly used to estimate the mode I fracture energy (J_{Ic}). The Compliance Calibration Method (CCM) is based on the establishment of the compliance versus crack length ($C=f(a)$) relationship and on the Irwin-Kies relationship

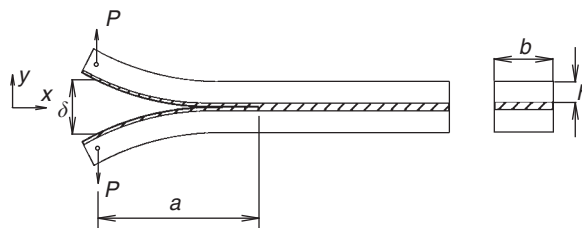$$J_{Ic} = \frac{P^2}{2b}\frac{dC}{da}$$

(5.16)

Figure 5.2 The DCB test.

where b is the specimen width and P the applied load. The Corrected Beam Theory (CBT) is based on the following equation [17]

$$J_{Ic} = \frac{3P\delta}{2b(a+|\Delta|)}$$ (5.17)

where δ is the applied displacement (Figure 5.2). The parameter Δ aims to correct the crack length in order to account for crack tip rotation and deflection effects and can be determined from a linear regression of $C^{1/3}$=f(a). It should be noted that both methods are based on monitoring of applied load and displacement as well as on the resulting crack length during its propagation. This last task is not easy to perform with the required accuracy especially when ductile adhesives are being characterized. Additionally, in these cases the pronounced fracture process zone ahead of the crack tip is responsible for a non-negligible amount of energy dissipation which is not accounted for when actual crack length is used as control parameter.

In order to overcome the referred difficulties, an equivalent crack length method based on specimen compliance and beam theory can be utilized. The objective is to use the current specimen compliance to estimate an equivalent crack length (a_e) by means of the beam theory. Following this procedure the monitoring of the crack length during the test is not necessary. Moreover, the influence of the non-negligible FPZ is indirectly included since it affects the current compliance which is used to estimate a_e. The application of the Timoshenko beam theory to the DCB specimen leads to the following equation [18]

$$C = \frac{8a^3}{E_1 bh^3} + \frac{12a}{5bhG_{13}}$$ (5.18)

where E_1 and G_{13} are the longitudinal and shear elastic properties of a general orthotropic material, and h the adherend thickness. In order to account for the influence of several parameters not included in the beam theory, like stress concentration in the vicinity of the crack tip, material variability between different specimens and the presence of the adhesive, an equivalent elastic modulus can be estimated from previous equation considering initial crack length a_0 and initial compliance C_0,

$$E_f = \left(C_0 - \frac{12(a_0+|\Delta|)}{5bhG_{13}}\right)^{-1} \frac{8(a_0+|\Delta|)^3}{bh^3}$$ (5.19)

where Δ is the correction to the initial crack length to account for the beam rotation at the crack tip. It can be calculated by a linear regression of $C^{1/3}=\mathrm{f}(a_0)$ considering three different initial crack lengths. Alternatively, the equations proposed by Wang and Williams [19] based on beam on elastic foundation assumptions can be used to estimate the crack length correction Δ_I which can be used instead of Δ in Eq. 5.19

$$\Delta_\mathrm{I} = h\sqrt{\frac{E_\mathrm{f}}{11G_{13}}\left[3 - 2\left(\frac{\Gamma}{1+\Gamma}\right)^2\right]}_{\text{being}} \quad \Gamma = 1.18\frac{\sqrt{E_\mathrm{f}E_3}}{G_{13}} \qquad (5.20)$$

To overcome the drawbacks intrinsic to crack monitoring during propagation, an equivalent crack length a_e can be calculated from the current compliance using Eq. 5.18. The solution of this cubic equation can be obtained using the Matlab® software and is presented in Appendix A. It should be emphasized that this procedure allows including the effect of beam root rotation and fracture process zone (FPZ), i.e., $a_\mathrm{e} = a + |\Delta| + \Delta a_\mathrm{FPZ}$, since these parameters affect the current compliance. The evolution of fracture energy as a function of equivalent crack length ($J_\mathrm{I}=\mathrm{f}(a_\mathrm{e})$) provides the resistance curve (*R*-curve) under mode I loading and can be obtained by combining Eqs. 5.16 and 5.18

$$J_\mathrm{I} = \frac{6P^2}{b^2h}\left(\frac{2a_\mathrm{e}^2}{h^2E_\mathrm{f}} + \frac{1}{5G_{13}}\right) \qquad (5.21)$$

The plateau of the *R*-curve corresponds to the critical fracture energy that characterizes the bonded joint. This method has some important advantages. The first one is the fact that the *R*-curve is obtained using only the data provided by the *P*–δ curve and does not require the monitoring of crack length which is prone to reading errors. Additionally, the effect of the fracture process zone is indirectly included in the calculations via current compliance. This is an important characteristic of this method, particularly when ductile adhesives are being characterized. Furthermore, since the elastic modulus is not a measured property but an estimated one considering the initial compliance and crack length, aspects like material variability and presence of adhesive are indirectly taken into account.

More details about the application of this methodology in the context of fracture characterization of bonded joints under mode I loading using the DCB test can be found in de Moura et al. [20].

5.3.2 End Notched Flexure (ENF) Test

Owing to its simplicity, the ENF test (Figure 5.3) is a serious candidate for standardization for the measurement of the fracture energy of bonded joints under pure mode II loading. It consists of a three-point bending test using a specimen with a pre-crack, thus leading to shear sliding between the specimen arms at the crack tip.

The classical methods presented for DCB test can also be used in this case. Thus, the CCM is based on Eq. 5.16 and the CBT, proposed by Wang and Williams [19], leads to

$$J_{IIc} = \frac{9P^2(a + |\Delta_{II}|)^2}{16b^2 E_1 h^3} \tag{5.22}$$

where Δ_{II} is a crack length correction to account for crack deflection. Wang and Williams [19] demonstrated that $\Delta_{II} = 0.42\Delta_I$, Δ_I being the correction for mode I obtained for the DCB test (Eq. 5.20). Both methods require crack length monitoring during its growth which is even more complicated to perform in these mode II loading tests. In this context, the implementation of a crack equivalent method similar to the one previously presented for DCB tests acquires special relevancy. The equation of compliance versus crack length in the ENF test using the Timoshenko beam theory leads to

$$C = \frac{3a^3 + 2L^3}{8E_1 bh^3} + \frac{3L}{10G_{13} bh} \tag{5.23}$$

The equivalent elastic modulus obtained from previous equation considering initial compliance and crack length becomes

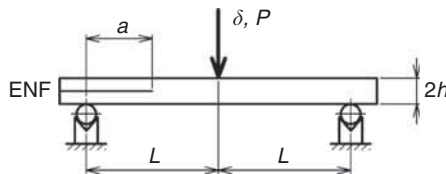$$E_f = \frac{3a_0^3 + 2L^3}{8bh^3}\left(C_0 - \frac{3L}{10G_{13} bh}\right)^{-1} \tag{5.24}$$

Figure 5.3 The ENF test.

The use of the equivalent elastic modulus (E_f) instead of the measured one (E_1) allows to account for several aspects not included in the beam theory equation, as the presence of adhesive, stress concentration at the crack tip and contact between the two arms in the pre-crack region. These aspects influence the specimen behaviour even in the elastic regime and are indirectly taken into account via E_f. During propagation, the equivalent crack length can be estimated from Eq. 5.23 as a function of current compliance C

$$a_e = a + \Delta a_{FPZ} = \left[\frac{C_c}{C_{0c}} a_0^3 + \frac{2}{3}\left(\frac{C_c}{C_{0c}} - 1 \right) L^3 \right]^{1/3} \tag{5.25}$$

where C_c and C_{0c} are given by

$$C_c = C - \frac{3L}{10 G_{13} bh} \; ; \; C_{0c} = C_0 - \frac{3L}{10 G_{13} bh} \tag{5.26}$$

The R-curve in mode II ($J_{II} = f(a_e)$) can now be obtained by combining Eqs. 5.16 and 5.23–5.26,

$$J_{II} = \frac{9 P^2 a_e^2}{16 b^2 E_f h^3} \tag{5.27}$$

The plateau of the R-curve defines the critical value of fracture energy under mode II loading. It is not necessary to monitor the crack length during propagation which is a remarkable advantage. In fact, this task is very difficult to perform with the required accuracy in mode II fracture tests, since the crack tends to propagate in closed manner. Additionally, the presence of a non-negligible FPZ is indirectly accounted for by means of current compliance. Under mode II loading adhesives usually develop larger FPZ relative to mode I tests, which emphasizes the relevancy of this method.

The application of the proposed procedure in the context of fracture characterization of bonded joints under mode II loading using the ENF test is detailed in de Moura et al. [21].

5.3.3   Determination of Cohesive Parameters of the Trapezoidal Law

The procedure described in previous Sections 5.3.1 and 5.3.2 permits to determine the fracture energy under pure loading modes (I and II). However, in order to define completely the trapezoidal

pure mode laws it is necessary to identify two additional parameters: the local cohesive strength $\sigma_{u,i}$ (i=I, II) and the displacement corresponding to the second inflexion point $\delta_{2,i}$ (i= I, II). These parameters can be determined by means of an inverse method. The fracture characterizations tests (DCB and ENF) are numerically simulated using the cohesive damage law whose circumscribed area is the respective fracture energy measured experimentally. The parameters $\sigma_{u,i}$ and $\delta_{2,i}$ are determined by fitting by an iterative procedure the numerical load-displacement curve to the experimental one. A genetic algorithm including an optimization strategy can be used [22]. However, previous studies [23] have shown that the model is not too sensitive to the value of $\delta_{2,i}$ in a pre-defined range of values. Consequently, this critical displacement was defined as being the one that induces, for the third part of the softening law, a symmetrical slope relative to the initial linear part. Therefore, only one parameter ($\sigma_{u,i}$) remains to be calculated by means of the inverse method which means that an iterative manual procedure can be straightforwardly applied. In effect, two or three iterations are typically sufficient to obtain a good agreement between load-displacement curves, thus leading to the definition of the respective local cohesive strength.

The described procedure was applied to fracture characterization of carbon-epoxy bonded joints under pure mode I (DCB test) and pure mode II (ENF test). The specimen dimensions for the DCB were (Figure 5.2): L= 120 mm, a_0 = 45 mm, $2h$ = 5.2 mm, b = 15 mm, t = 0.2 mm. For the ENF specimens the only difference was the specimen length $2L$ = 200 mm (Figure 5.3). The adherends (unidirectional 0° lay-ups with sixteen layers of TEXIPREG HS 160 RM from SEAL®, Legnano, Italy whose elastic properties are listed in Table 5.1) were bonded with the adhesive Araldite® 2015 (Young modulus, E=1850 MPa and Poisson ratio v=0.3). The bonded surfaces were polished with sandpaper and cleaned with acetone. Then, a 0.2 mm calibrated steel strip was inserted between the two specimen arms to guarantee the adhesive thickness. The next stage was pouring the adhesive, assembling and holding it with pressure. The adhesive was cured at room temperature for five days.

The average trapezoidal cohesive laws for each pure mode were obtained by means of the above described inverse method and the fundamental parameters are presented in Table 5.2. The

Table 5.1 Elastic properties of carbon-epoxy lamina [20].

E_1=1.09E+05 MPa	v_{12}=0.342	G_{12}=4315 MPa
E_2=8819 MPa	v_{13}=0.342	G_{13}=4315 MPa
E_3=8819 MPa	v_{23}=0.380	G_{23}=3200 MPa

E_1, E_2, E_3 – Young's moduli
v_{12}, v_{13}, v_{23} – Poisson's ratios
G_{12}, G_{13}, G_{23} – Shear moduli

Table 5.2 Cohesive parameters under pure modes I and II.

	J_{ic} (N/mm)	$\sigma_{u,i}$ (MPa)	$\delta_{2,i}$ (mm)
Mode I	0.43	23	0.0187
Mode II	4.7	22.8	0.171

J_{ic} – Fracture energy in the mode i (i=I, II)
$\sigma_{u,i}$ – Local strength in the mode i (i=I, II)
$\delta_{2,i}$ – Relative displacement at the second inflexion point of the trapezoidal cohesive law in the mode i (i=I, II)

corresponding global cohesive laws for both modes are presented in Figure 5.4. More details about these procedures and respective results can be found in [20, 21].

5.3.4   Bonded Joints Strength Prediction

In order to verify the adequacy of the proposed methodology to predict the strength of bonded joints, experimental tests on single-lap carbon-epoxy bonded joints under tensile load were performed. The materials of the adherends (thickness of 2.5 mm) as well as the adhesive were the same as used in the fracture characterization tests. In addition, the adhesive thickness was also the same (t=0.2 mm) in order to reproduce the test conditions of the fracture characterization tests. The specimens had a useful length of 240 mm and a width of 15 mm. Eight different overlap lengths (ranging between 10 and 80 mm) were considered. Five specimens of each case were tested under displacement control
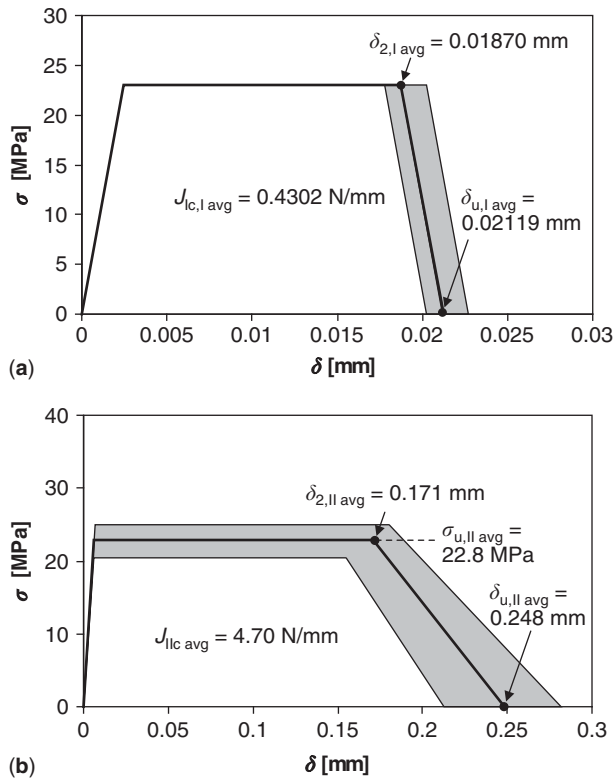
Figure 5.4 Cohesive laws; a) Pure mode I loading; b) Pure mode II loading.

and the maximum load was registered and used to define the joint strength. The failure occurred within the adhesive layer (cohesive failure) in all cases.

The joints were also simulated numerically by considering the trapezoidal cohesive mixed-mode damage model described in Section 5.2. The mesh was refined in the overlap region and its vicinity (element length of 0.4 mm provided converged results) in order to capture accurately the stress concentrations that arose in these regions. The cohesive pure mode laws in mode I and mode II used in the simulations were the ones determined by the procedure described in previous Sections 5.3.1, 5.3.2 and 5.3.3. Figure 5.5 presents the evolution of experimental and numerical results. It can be concluded that generally good agreement was obtained which demonstrates the adequacy of the proposed methodology.
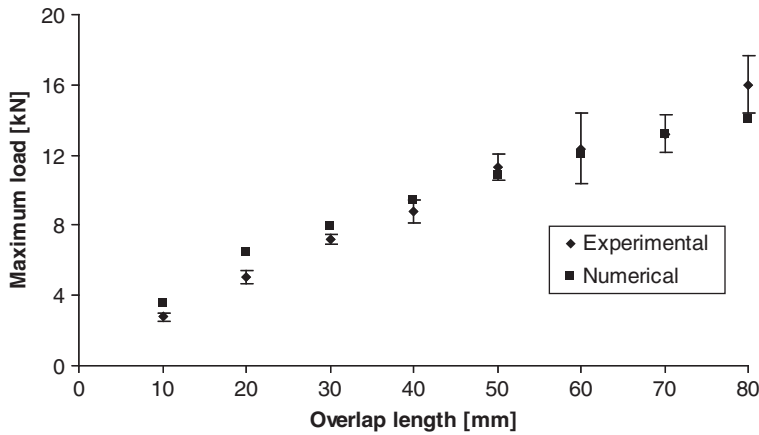
Figure 5.5 Comparison between numerical (cohesive zone model) and experimental single-lap joint strengths in terms of maximum loads as a function of overlap length.

5.4   Continuum Damage Models

The application of cohesive models described in previous section neglects the adhesive thickness. This can constitute a limitation specially when thick adhesive layers are used and asymmetrical crack propagation with different paths along adhesive thickness occur. In these cases, typical pure mode cases can be affected by the presence of some mode mixity due to asymmetrical crack growth [24], which can alter the expected mechanical behaviour. Also, it is known that adhesive thickness can influence the mechanical properties of the joint [16]. In order to overcome these drawbacks continuum damage models can be used. In these models the material properties degradation occurs inside the solid elements that are used to simulate the adhesive. The progressive damage is computed considering the damage onset and propagation criteria in the formulation of solid elements. Typically, this is carried out through a user subroutine implemented in standard software, where the material properties are degraded according to the selected criterion. In the following, a triangular softening relationship between stresses and strains is implemented in the ABAQUS Standard® software via UMAT user subroutine. The bilinear pure-mode law (Figure 5.6) was implemented in two-dimensional solid elements used to simulate the adhesive behaviour [25].
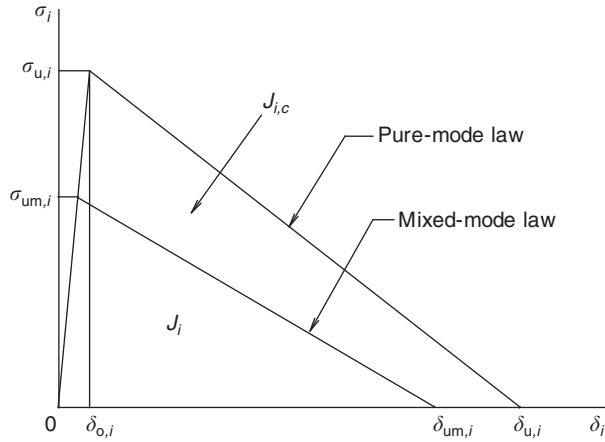
Figure 5.6 Bilinear pure-mode and mixed-mode laws.

In this pure mode model damage onset occurs when local strength ($\sigma_{u,i}$, i = I, II) is reached. Damage growth takes place when the respective fracture energy defined by the triangular area circumscribed by cohesive pure-mode law

$$J_{ic} = \frac{\sigma_{u,i}\varepsilon_{u,i}l_{c,i}}{2}, i = \mathrm{I,II} \tag{5.28}$$

is dissipated at a given integration point. A characteristic length $l_{c,i}$ is used to establish the relationship between the displacement (δ_i) and the corresponding strain at the integration points of the solid elements, i.e., $\varepsilon_i = \delta_i/l_{c,i}$. This parameter corresponds to the length of influence of each integration point and physically can be viewed as the length at which the material behaves homogeneously. After the ultimate stress $\sigma_{u,i}$ is attained, the stress–strain softening relationship becomes

$$\sigma = (\mathrm{I} - \mathrm{D})\mathrm{C}\varepsilon \tag{5.29}$$

where C is the stiffness matrix of the undamaged material in the orthotropic directions and D is the matrix containing the damage parameter d_i in the direction corresponding to the selected pure mode i

$$_i = \frac{\delta_{u,i}(\delta_i - \delta_{o,i})}{\delta_i(\delta_{u,i} - \delta_{o,i})} \tag{5.30}$$

where δ_i, $\delta_{o,i}$ and $\delta_{u,i}$ represent, respectively, the current, onset and ultimate relative displacements. The last quantity can be easily obtained from Eq. 5.28 as a function of previously known J_{ic} and $\sigma_{u,i}$. The damage parameter varies between zero (undamaged material, i.e., $\delta_i \leq \delta_{o,i}$) and unity (complete material failure, i.e., $\delta_i \geq \delta_{u,i}$).

The application of the continuum damage model to bonded joints requires the development of a mixed-mode model (Figure 5.6), since structural bonded joints are frequently subjected to mixed-mode loading. Damage onset is detected by means of a quadratic stress criterion

$$\left(\frac{\sigma_I}{\sigma_u}\right)^2 + \left(\frac{\sigma_T}{\sigma_u}\right)^2 + \left(\frac{\tau}{\tau_u}\right)^2 = 1 \text{ if } \sigma_I > 0$$
$$\tau = \tau_u \text{ if } \sigma_I < 0 \tag{5.31}$$

σ_I, σ_T being the normal and τ the shear stresses (Figure 5.7), and σ_u, τ_u the corresponding ultimate values. In addition to the shear mode II (τ) and normal mode I (σ_I), another normal component (σ_T) parallel to crack direction is considered. This component is generally known as the T-stress component and has been shown to play an important role when crack growth under mixed-mode loading is concerned [26] and in the size and shape of the plastic zone [27]. Under compressive stresses (i.e., $\sigma_I < 0$) it is assumed that damage is dictated only by the shear stress component and a pure mode II loading is considered (second Eq. 5.31).

The first Eq. 5.31 can be used to obtain an equivalent mode I ultimate stress causing damage initiation. With this aim the following ratios are considered

$$a_s = \frac{\sigma_T}{\sigma_I} \; ; \; \beta_s = \frac{|\tau|}{\sigma_I} \tag{5.32}$$
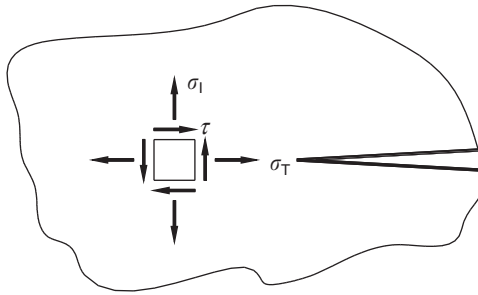
Figure 5.7 Adhesive layer stress components in the vicinity of the crack tip.

Combining Eqs. 5.32 and the first Eq. 5.31 gives

$$\sigma_{\text{eI}} = \frac{\sigma_{\text{u}}\tau_{\text{u}}}{\sqrt{\tau_{\text{u}}^2(1 + a_{\text{s}}^2) + \beta_{\text{s}}\sigma_{\text{u}}^2}} \tag{5.33}$$

which corresponds to the equivalent stress that, taken into account the mode ratios (Eqs. 5.32) present in the problem, leads to damage initiation. The damage parameter (Eq. 5.30) under mixed-mode loading should be defined as a function of equivalent mixed-mode displacements instead of the pure mode ones. In this context, the relative displacement components in each mode ($\delta_{\text{om,I}}$ and $\delta_{\text{om,II}}$) corresponding to damage initiation can be obtained using the Hooke's law and Eq. 5.32

$$\delta_{\text{om,I}} = \frac{\sigma_{\text{eI}}}{E}(1 - va_{\text{s}})l_{\text{c}}$$

$$\delta_{\text{om,II}} = \frac{2\sigma_{\text{eI}}(1 + v)}{E}\beta_{\text{s}}l_{\text{c}} \tag{5.34}$$

where E and v are the elastic modulus and Poisson's ratio, respectively. The equivalent relative displacement at damage onset is given by

$$\delta_{\text{om}} = \sqrt{\delta_{\text{om,I}}^2 + \delta_{\text{om,II}}^2} = \frac{\sigma_{\text{eI}}}{E}\sqrt{(1 - va_{\text{s}})^2 + 4\beta_{\text{s}}^2(1 + v)^2}\, l_{\text{c}} \tag{5.35}$$

The linear energetic criterion

$$\frac{J_{\text{I}}}{J_{\text{Ic}}} + \frac{J_{\text{II}}}{J_{\text{IIc}}} = 1 \tag{5.36}$$

is utilized to simulate damage growth. The two components of energy that contribute to mixed-mode present in the problem are given by (Figure 5.6)

$$J_{\text{I}} = \frac{\sigma_{\text{I}}\delta_{\text{um,I}}}{2} \; ; \; J_{\text{II}} = \frac{|\tau|\delta_{\text{um,II}}}{2} \tag{5.37}$$

where σ_{I} and τ are the limiting stresses in each mode ($\sigma_{\text{um},i}$ in Figure 5.6) at damage initiation and $\delta_{\text{um,I}}$, $\delta_{\text{um,II}}$ the ultimate relative displacements in each mode. Considering a relative displacement ratio

$$\beta_{\text{d}} = \frac{\delta_{\text{II}}}{\delta_{\text{I}}} \tag{5.38}$$

and substituting Eqs. 5.37 into 5.36 gives

$$\delta_{um} = \sqrt{\delta_{um,I}^2 + \delta_{um,II}^2} = \frac{2\sqrt{(1+\beta_d^2)^2}}{\sigma_{eI}\left(\dfrac{1}{G_{Ic}} + \dfrac{\beta_d\beta_s}{G_{IIc}}\right)} \qquad (5.39)$$

which establishes the ultimate equivalent mixed-mode I+II displacement leading to complete failure as a function of the ratios of relative displacements and stresses that define the mode-mixity present in the problem. The equivalent mixed-mode I+II quantities $(\delta_m, \delta_{om}, \delta_{um})$ are employed in Eq. 5.30 to estimate the damage parameter d_m, used in Eq. 5.29 to simulate a progressive damage under mixed-mode I+II loading. It should be noted that the mode-mixity induced by the applied load is taken into account through the mode ratio parameters (β_d and β_s).

### 5.4.1   Application to DCB Test

The application of the continuum damage model to bonded joints allows considering the presence of the adhesive in a more proficient way than in cohesive modelling. In order to verify the consequences of this aspect, the model was applied to the DCB test considering an adhesive thickness t equal to 0.2 mm (Figure 5.8). The other specimen dimensions were the ones described in previous Section 5.3.3.

Considering the procedure described in Section 5.3.1 and the properties listed in Table 5.1 (local strength and fracture energy) the following resistance curve (R-curve) was obtained (Figure 5.9).

Since the fracture energy is normalized by the inputted one it can be straightforwardly concluded that a slight overestimation of the inputted value takes place during the self-similar crack
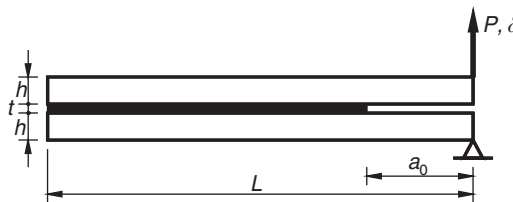
**Figure 5.8** Schematic representation of the DCB test simulated using the continuum damage model.
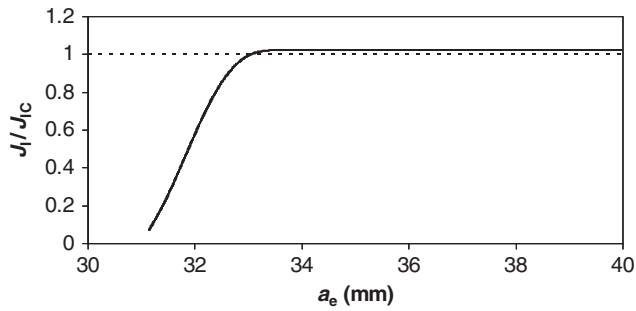
Figure 5.9 *R*-curve of the DCB test. The horizontal line ($J_I/J_{Ic}=1$) identifies the value inputted in the model.

propagation observed by the horizontal plateau of the *R*-curve. In order to explain this result the evolution of the damage process inside the adhesive layer was captured for four different steps of the loading process (Figure 5.10). The crack length was defined by the integration points where the failure process had been completed and normal stresses had vanished. The FPZ region comprises the integration points that are in the softening region (Figure 5.6), which means that damage is already present although normal stresses still exist.

It can be verified that crack tends to develop close to an interface. Additionally, the fracture process zone is distributed asymmetrically being more concentrated towards an interface. These observations are in agreement with the ones obtained by Gonçalves et al. [24], concerning the propagation occurring close to an interface. It was verified in [24] that stress concentration arises at interfaces over the mid-plane of the adhesive due to localized mismatch between different materials (adherend and adhesive). These aspects mean that damage grows asymmetrically, thus leading to a localized mixed-mode loading instead of the intended pure mode I. The presence of some mode II loading induced by asymmetrical propagation justifies the slight overestimation of the fracture energy and highlights the importance of the continuum damage models when applied in the context of bonded joints. Effectively, the slight overestimation that results for $t=0.2$ mm will increase with adhesive thickness and this phenomenon is not able to be captured with cohesive modelling.

Another interesting aspect is the fact that the FPZ region ahead of crack tip maintains approximately the same shape and size in
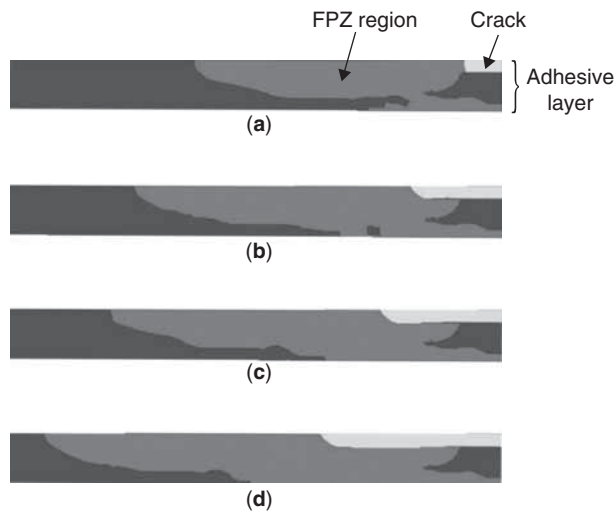
Figure 5.10 Evolution of damage (crack and FPZ region) inside the adhesive layer in the DCB test. Figures a-d present four steps of the evolution of the crack and the FPZ region inside the adhesive.

all steps (Figure 5.10). This circumstance reveals a self-similar crack growth process which leads to a plateau in the *R*-curves (Figure 5.9).

5.4.2   Application to Single-Lap Joints

In order to verify the performance of the mixed-mode I+II continuum damage model proposed in the previous section, the model was applied to predict strength of single-lap bonded joints. The continuum damage model was implemented in 8-node plane stress solid elements used to simulate the adhesive behaviour (Figure 5.11).

The experimental results used to validate the numerical results are the ones presented in Section 5.3.4. Generally, good agreement was obtained between the numerical and experimental results as can be seen in Figure 5.12. This demonstrates the adequacy of the model with the advantage that it includes the presence of the adhesive. Additionally, it is possible to simulate crack propagation along different paths inside the adhesive, although in this particular case this aspect is not relevant owing to low adhesive thickness (*t*=0.2 mm).
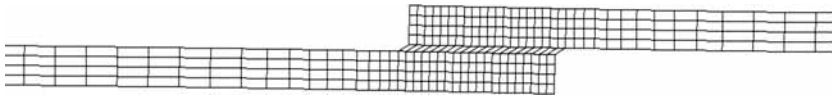
Figure 5.11 Detail of the mesh used and the respective deformation in a single-lap bonded joint.
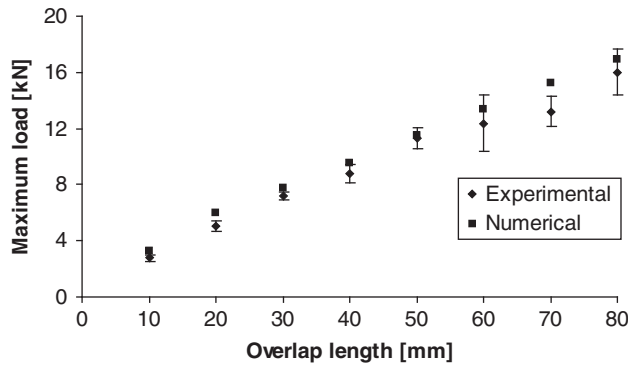
Figure 5.12 Comparison between numerical (continuum damage model) and experimental single-lap joint strengths in terms of maximum loads as a function of overlap length.

5.5 Conclusion

Adhesive bonded joints are being increasingly applied in critical structural applications. Therefore, more challenging design methods accounting for several specificities inherent to these crucial applications should be considered. Cohesive and continuum mixed-mode damage models emerge as efficient design tools when applied to bonded joints strength prediction. Both methods are based on stress based criteria to deal with damage initiation and fracture mechanics approaches to simulate damage growth, thus overcoming the drawbacks of each criterion and gaining benefit of their advantages.

In this context, a trapezoidal cohesive mixed-mode I+II cohesive damage law adequate for the simulation of ductile adhesives was presented. The respective cohesive parameters were estimated by means of an inverse method applied to the DCB and ENF fracture characterization tests for pure modes I and II, respectively. The inverse method is based on an iterative procedure with the aim of

fitting the numerical and experimental load-displacement curves, thus defining the constitutive cohesive laws in the two modes. Owing to difficulties intrinsic to crack length monitoring during its propagation in the DCB and ENF tests, crack equivalent based methods were applied. Comparison between numerical and experimental results for single-lap joints strength under tensile loading revealed good performance of the model.

A continuum bilinear mixed-mode I+II damage model was also presented. This method is based on the implementation of a damage softening law inside solid elements which allows to account for the presence of the adhesive in a more efficient way relative to cohesive models. Details, such as asymmetrical crack and fracture process zone growth and their influence on the measured fracture properties are well managed by the continuum damage models. The model was applied to predict single-lap bonded joints strength under tensile loading and showed good performance when compared to experimental results.

Appendix A

Eq. 5.18 can be expressed as,

$$\alpha a_e^3 + \beta a_e + \gamma = 0 \qquad \text{(A.5.1)}$$

where the coefficients α, β and γ are

$$\alpha = \frac{8}{bh^3 E_f}; \quad \beta = \frac{12}{5bhG_{13}}; \quad \gamma = -C \qquad \text{(A.5.2)}$$

Using the Matlab® software and keeping only the real solution we have,

$$a_e = \frac{1}{6\alpha} A - \frac{2\beta}{A} \qquad \text{(A.5.3)}$$

with

$$A = \left(\left(-108\gamma + 12\sqrt{3\left(\frac{4\beta^3 + 27\gamma^2 \alpha}{\alpha} \right)} \right) \alpha^2 \right)^{\frac{1}{3}} \qquad \text{(A.5.4)}$$

References

1. J.A. Harris and R.D. Adams. *Int. J. Adhesion Adhesives* 4, 65–78 (1984).
2. K. Ikegami, T. Takeshita, K. Matsuo and T. Sugibayashi. *Int. J. Adhesion Adhesives* 10, 199–206 (1990).
3. S.J. Lee and D.G. Lee. *J. Adhesion* 40, 1 (1992).
4. A. Towse, R.G.H. Davies, A. Clarke, M.R. Wisnom, R.D. Adams and K.D. Potter, in: *Proceedings of the 4th International Conference on Deformation and Fracture of Composites,* Institute of Materials, London, pp. 479–483 (1997).
5. S.J. John, A.J. Kinloch and F.L. Matthews. *Composites* 22, 121–127 (1991).
6. X. Zhao. Stress and failure analysis of adhesively bonded lap joints, PhD thesis, Department of Mechanical Engineering, University of Bristol, UK (1991).
7. A.J. Kinloch, *Adhesion and Adhesives: Science and Technology*, Chapman & Hall, London (1987).
8. E.J. Ripling, S. Mostovoy and R.L. Patrick, in: *Adhesion*, F.W. Reinhart (Ed.), ASTM STP 360, ASTM, Philadelphia, PA (1963).
9. Y. Mi, M.A. Crisfield, G.A.O. Davies and H.B. Hellweg. *J. Composite Mater.* 32, 1246–1272 (1998).
10. Z. Petrossian and M.R. Wisnom. *Composites Part A*, 29A, 503–515, (1998).
11. M.F.S.F. de Moura, J.P.M. Gonçalves, A.T. Marques and P.M.S.T. de Castro. *Composite Struct.* 50, 151–157 (2000).
12. J.P.M. Gonçalves, M.F.S.F. de Moura, A.G. Magalhães and P.M.S.T. de Castro. *Fatigue Fract. Engng. Mater. Struct.* 26, 479–486 (2003).
13. Q.D. Yang, M.D. Thouless and S.M. Ward. *J. Mech. Phys. Solids* 47, 1337–1353 (1999).
14. T. Andersson and U. Stigh. *Int. J. Solids Struct.* 41, 413–434 (2004).
15. R.D.S.G. Campilho, M.F.S.F. de Moura, A.M.G. Pinto, J.J.L. Morais and J.J.M.S. Domingues. *Composites Part B* 40, 149–157 (2009).
16. D.B. Lee, T. Ikeda, M. Miyazaki and N.S. Choi. *J. Eng. Mater. Technol.* 126, 14–18 (2004).
17. M.F.S.F. de Moura, A.B. Pereira and A.B. de Morais. *Fatigue Fract. Engng. Mater. Struct.* 27:759–766 (2004).
18. M.F.S.F. de Moura, J.J.L. Morais and N. Dourado. *Eng. Fract. Mech.* 75, 3852–3865 (2008).
19. Y. Wang and J.G. Williams. *Composites Sci. Technol.* 43, 251–256 (1992).
20. M.F.S.F. de Moura, R.D.S.G. Campilho and J.P.M. Gonçalves. *Composites Sci. Technol.* 68, 2224–2230 (2008).
21. M.F.S.F. de Moura, R.D.S.G. Campilho and J.P.M. Gonçalves. *Int. J. Solids Struct.* 46:1589–1595 (2009).
22. N. Dourado, S. Morel, M.F.S.F. de Moura, G. Valentin and J. Morais, *Composites Part A* 39, 415–427 (2008).
23. M.F.S.F. de Moura, J.P.M. Gonçalves, J.A.G. Chousal and R.D.S.G. Campilho., *Int. J. Adhesion Adhesives* 28, 419–426 (2008).
24. J.P.M. Gonçalves, M.F.S.F. de Moura and P.M.S.T. de Castro. *Int. J. Adhesion Adhesives* 22, 357–365 (2002).
25. M.F.S.F. de Moura and J.A.G. Chousal. *Int. J. Mech. Sci.* 48, 493–503 (2006).
26. D.J. Smith, M.R. Ayatollahi and M.J. Pavier. *Fatigue Fract. Engrg. Mater. Struct.* 24 137–150 (2001).
27. S.G. Larsson and A.J. Carlson. *J. Mech. Phys. Solids* 21, 263–277 (1973).